

## Response

### 1. Referees 1 & 2 Comments

Referee 1: *The study is an important contribution to the ongoing efforts to evaluate the importance of nitrous oxide fluxes in the permafrost regions. The authors have considered in details the methodological aspects of the airborne EC method they applied...The footprint analyses here also indicated areas with negligible emissions and areas with high nitrous oxide emissions.*

Referee 2: *Overall, the analytical technique and estimation of N<sub>2</sub>O flux based on EC Method are well described with plenty of details. The analytical precision of N<sub>2</sub>O mixing ratios seems satisfying for airborne measurement, and uncertainty in flux estimations has been also discussed.*

1.1 Response to Referees: We appreciate the referees' affirmation of the techniques and uncertainty analysis on which we base our conclusions.

1.2 Change to Manuscript: None.

### 2. Referees 1 & 2 Comments

Referee 1: *To get such a high mean emission rate shown here by the EC, the emissions from the high-emitting areas have to be very high. Would be excellent if the authors could get some published or non-published data on nitrous oxide emissions in the region based on chamber measurements or determined by a gas gradient approach based on nitrous oxide content in soil. This data could then be upscaled by estimating the total coverage of the high emitting areas. If the nitrous emissions from these analyses are in the same range as the mean emission rate here, this could confirm the results obtained by EC.*

Referee 2: *However, given the unexpectedly high N<sub>2</sub>O flux, it remains a question to us how realistic flux data we could obtain based on these airborne measurements within limited time scales. Although this approach has been tested for CH<sub>4</sub>/H<sub>2</sub>O with a near-by EC tower (Sayres et al., 2017), spatial variabilities in N<sub>2</sub>O fluxes could largely differ. Therefore, more ground-based fluxes data in the near region by EC tower or chamber measurements are necessary to confirm the applicability of this technique. Alternatively, if N<sub>2</sub>O emission factors or edaphic parameters are available in this or other similar regions, a ground-based model estimation of N<sub>2</sub>O fluxes separating landscape elements may strengthen the whole manuscript.*

2.1 Response to Referees: Indeed the high-emitting "hot-spots" have to be quite prominent to affect the overall average. The nature of an airborne study is to provide a spatial survey of the prevalence and spatial distribution of such high-emission locations along with any other distributed sources in an area difficult of access. The reviewer characterizes the high spatial variation of N<sub>2</sub>O flux to be well known from chamber methods. The significance of our result, in addition to confirming the spottiness, is to find such hot spots and other sources of N<sub>2</sub>O to be sufficiently strong and/or numerous over landscape and larger scales on the North slope to add up to average N<sub>2</sub>O emission comparable to that found in the tropics.

To our knowledge, established emission factors do not currently exist for permafrost N<sub>2</sub>O emissions. No significant emissions were reported from any permafrost land class until 2009, when researchers identified bare peat circles as potential emitters of

significant amounts of  $\text{N}_2\text{O}$ . Several other studies (cited in the manuscript) have since come out reinforcing the notion that  $\text{N}_2\text{O}$  could be significant. However, these are mostly laboratory studies, soil  $\text{N}_2\text{O}$  observations, and metagenomic analyses, which do not translate to emission factors. The first results from this airborne approach reinforce the need for continued and enhanced examination, both spatially and temporally extensive, in the arctic. We seek to publish the significant result we've observed on a landscape-scale to help motivate future studies that can provide the confirmation sought in Referee 1's comment.

In response to Referee 2, we agree that the spatial variability for  $\text{N}_2\text{O}$  could be different -- as demonstrated by our measurements. However, that does not necessitate comparative ground-based measurements catered specifically to  $\text{N}_2\text{O}$ . Comparison with another measurement technique would only be necessary if there are concerns about our primary method. No concerns were given. As stated in the manuscript, our comparison with a nearby tower demonstrates that our instrument is capable of measuring airborne fluxes of gases. We also calibrated our EC system both in a wind tunnel and during the campaign. From the perspective of making trace gas flux measurements then, the only difference between  $\text{CH}_4$ ,  $\text{H}_2\text{O}$ , and  $\text{N}_2\text{O}$  is a different absorption feature on our spectra. Since we demonstrate that the template of our EC system works, all that is left is making sure the  $\text{N}_2\text{O}$  sensor works properly. We have done this, both in lab and in flight, and furthermore, performed an uncertainty analysis on the  $\text{N}_2\text{O}$  flux data, which includes a comprehensive ogive plot. The referee seems satisfied by this as shown in Comment 1 above.

Separately, there is an issue regarding Referee 2's recommendation that we use chambers to confirm airborne measurements. For an airborne measurement to correspond to a fixed surface measurement their footprints must correspond. A chamber measures the same small patch (typical size for a chamber is  $\sim 1 \text{ m}^2$ ). By contrast, the minimum spatial coverage of an aircraft measurement, determined by the largest scale of atmospheric turbulence, is closer to  $6 \text{ km}^2$ . For the footprints from the two methods to correspond, the aircraft track must lie over a homogeneous surface of area  $6 \text{ km}^2$  having the same character as that being sampled by the chamber (and the chamber's 1-square-meter footprint must accurately represent the 6-square-kilometer surface covered by the aircraft's measurements). For  $\text{CH}_4$  or  $\text{CO}_2$  such a surface can be identified by remote sensing. As discussed above, however, no comparable surface classification for  $\text{N}_2\text{O}$  is available to our or, presumably, to the referees' knowledge. An EC tower would sample a larger surface area than a chamber but would be subject to the same issues in establishing a common footprint with aircraft for  $\text{N}_2\text{O}$ .

Therefore, while we do agree that comparison with a tower for  $\text{N}_2\text{O}$  specifically 'would be excellent' as Referee 1 states, we disagree that it's necessary as Referee 2 suggests. Having said that, we do state on Page 9/lines 20-21 that this is a stepping stone where future research would provide that ground comparison. Considering no one is currently doing this, we strongly believe publishing this information for the scientific community to see is an important step to motivate the community to look further into what's going on here. This is especially true since several chamber-based

publications have already recently been published suggesting the community's assumptions about permafrost N<sub>2</sub>O emissions may need to be refined.

Finally, we agree with Referee 2 that we cover a smaller time scale than a longer-term ground-based measurement. But accordingly, we restrain our extrapolation to the month of August instead of the entire summer precisely because of our shorter time scale.

2.2 Change to Manuscript: None.

3. Referee 1 Comment

*Page 2/line 1 Change the text to “. . .However, recent in situ measurement of permafrost soils in Russian tundra and northern Finland (Repo et al. 2009; Marushchak et al. 2011)”*

3.1 Response to Referee: We agree with the suggestion and have changed the manuscript accordingly.

3.2 Change to Manuscript: The text was changed as Referee 1 suggested (Page 2/line 3).

4. Referee 1 Comment

*Page 2/lines 10-16 The discussion on the flux data generated by chamber method could be modified to state that there are both disadvantages and benefits using chamber method for the gas fluxes. By the chambers we can catch efficiently the various functional surfaces, even very small. So, we can get knowhow on the soil and vegetation related factors affecting gas fluxes. To obtain landscape or regional fluxes by chambers for permafrost regions, accurate distribution of the functional surfaces is required. This can be done using e.g. satellite images (e.g. Treat et al. 2018. Global Change Biology, Doi: 10.1111/gcb14421).*

4.1 Response to Referee: Thank you for pointing this out. We did not bring up the spatial limitation of the chamber method to suggest that method has no benefits. Rather, our goal was to point out a gap in the research that an alternative method could help fill in – our method specifically. We did point to several benefits of chamber studies on Page 2/line 10. Still, we appreciate that a reader could get the impression we might be offering airborne EC as a replacement method. That is not what we are doing. Airborne EC complements the chamber method and ground-based measurements in general. We will alter the text to better convey this sentiment.

As for the latter part of the comment, it's true that research teams perform quite spatially extensive extrapolations from chamber measurements to get a landscape-scale estimate of some trace gas emissions. Treat et al. 2018, the paper the referee cites, examines this method, and the potential pitfalls of using it, for CO<sub>2</sub> and CH<sub>4</sub>. It does not for N<sub>2</sub>O. This is probably because permafrost N<sub>2</sub>O emissions have had significantly less research effort dedicated to them. Unlike the EC tower network that exists to varying extent for CO<sub>2</sub> and CH<sub>4</sub>, there is not a single EC tower that provides consistent, long-term measurements of permafrost N<sub>2</sub>O emissions. Chamber studies are also quite sparse. While research effort sufficient for discussion of this type of extrapolation may eventually be put forth for N<sub>2</sub>O, such discussion feels more relevant for CO<sub>2</sub> and CH<sub>4</sub> at this time.

We mentioned that Treat et al. discuss potential pitfalls of this type of extrapolation in their paper. We'd like to touch on that again as a way to further emphasize how it might be premature to discuss these types of extrapolations for permafrost N<sub>2</sub>O. One of Treat's main messages is that satellite images can cause severe underestimations if an insufficient resolution is chosen. They've found that you need a better spatial resolution for CH<sub>4</sub> than for CO<sub>2</sub> because CH<sub>4</sub> emissions are more spatially variable. Without proper resolution, the CH<sub>4</sub> emissions are severely underestimated (by up to 65%). N<sub>2</sub>O is considered much more variable and spotty than CH<sub>4</sub>. We can imagine the spatial resolution therefore needs to be even better to extrapolate N<sub>2</sub>O emissions, but it's unknown what this resolution should be or whether traditional satellite maps could properly accomplish this (the land cover map we used has the recommended 30 m x 30 m resolution for CH<sub>4</sub>). Our presented results involved no extrapolation and, therefore, no need to make assumptions about the characteristics of a particular land class as it relates to N<sub>2</sub>O or to worry about potential issues with the resolution of satellite images used to make the extrapolations. Instead, we obtained a landscape-scale estimate from hours of airborne measurements spanning hundreds of square kilometers of the Arctic. There are certainly advantages of the chamber method over airborne EC, as we have now more explicitly stated. However, obtaining a landscape-scale estimate is not one of them.

4.2 Change to Manuscript: Page 2/lines 14-23 changed to "The past studies on permafrost N<sub>2</sub>O emissions have provided insight into the mechanisms of the gas's production and subsequent release into the atmosphere. The studies have been either laboratory studies or ground-based chamber studies. In general, chamber studies have the advantage of observing the same site for relatively long time periods. Additional variables (e.g. pH, water saturation) can be monitored, too, which are crucial to understanding how that environment might influence the observed extent of N<sub>2</sub>O emissions. However, each chamber covers around 1 m<sup>2</sup>, and a feasible chamber study can only entail a limited number of sites. Consequently, past observations have covered extremely small areas – less than 50 m<sup>2</sup> (Repo et al. 2009; Marushchak et al. 2011; Yang et al. 2018). Therefore, the landscape scale of this phenomenon remains unknown, let alone the regional and continental scales. Landscapes deemed vulnerable to thaw-induced N<sub>2</sub>O emissions, permafrost and thermokarst regions, cover about one fourth of the Arctic/sub-Arctic (Voigt et al. 2017). One of those vulnerable areas is the Alaskan North Slope, which is the focus of this study. To get a landscape-scale estimate of the magnitude of permafrost N<sub>2</sub>O emissions during late summer, we measured N<sub>2</sub>O fluxes over the North Slope in late August 2013 using the airborne eddy covariance (EC) technique."

We also modified the text in the Conclusion (Page 9/lines 14-16), to read: "Importantly, we corroborate these findings in a complementary way: by observing fluxes on a landscape scale rather than the much smaller-scale soil plots in chamber studies, which are intended more to understand temporal representativeness and mechanisms of N<sub>2</sub>O production."

5. Referee 2 Comment

*Page 2, Line 10-16: The authors argued that chamber measurement or lab studies cover small spatial scales. However, the airborne measurements cover only short time periods. Perhaps a little more background on spatio-temporal variabilities in N<sub>2</sub>O fluxes from permafrost?*

5.1 Response to Referee: The reported average presented in our manuscript represents, in total, a little under 10 hours of airborne measurements across the North Slope semi-randomly sampled over the span of a week. To give an estimate for the entire month of August, we therefore extrapolate our data by an order of 100. By comparison, a typical chamber study covers an area around 10,000,000 times smaller than our spatial coverage. We agree that we are temporally limited, but the spatial limitation for chambers seems more severe. Regardless, our point was not to suggest airborne EC is better than chamber studies, merely that it's more appropriate for establishing a landscape-scale estimate. We have modified the text to better convey this.

5.2 Change to Manuscript: Please see changes in Comment Response 4

6. Referee 2 Comment

*Page 2, Line: 17-20: Much of the detailed information on flight campaign could be put in M&M.*

6.1 Response to Referee: Most of that text has been moved to the first paragraph of the Methods section.

6.2 Change to Manuscript: Except for the last sentence, Page 2, Lines 17-20 were all moved to the first paragraph of Methods section (Page 2, Line 35-37). The text was also slightly modified to better flow with the text following its new location.

7. Referee 2 Comment

*Page 5, Line 1, equation (3): I think that running flux method (RFM, Sayres et al. 2017) was used for N<sub>2</sub>O flux estimations in this manuscript. However, Sayres et al. (2017) suggested advantage of flux fragment method (FFM) against RFM in their airborne EC CH<sub>4</sub> study. Also, they claimed that FFM can isolate flux contributions from individual surface land classes. Please explain it.*

7.1 Response to Referee: The running flux method was not used for N<sub>2</sub>O flux estimations presented in Table 2 of this manuscript. Equation (3) is the general equation for airborne EC fluxes, not an equation specific to RFM. We don't use FFM either. We opted instead for the more robust approach of averaging over entire flights in order to focus on the overarching landscape and to present simpler, more statistically sound results.

We do, however, use RFM to determine the values for the data in Figure 6. RFM is an application of equation (3), as described in Page 7/lines 9-10 of the ACPD manuscript (note we avoid using the term 'RFM' in an effort to minimize jargon in the manuscript). Regarding FFM versus RFM, Sayres et al. 2017 only suggests advantage of FFM over RFM under certain circumstances. They do not assert FFM has an overall

advantage (some of the authors of that publication also author this manuscript). The goal of Figure 6 is to illustrate the spottiness of N<sub>2</sub>O emissions, and RFM is better suited for that purpose.

7.2 Change to Manuscript: On Page 5/line 2, we changed the equation (3) description from 'standard equation' to 'general equation' to better clarify this is not an equation specific to RFM or FFM.

#### 8. Referee 2 Comment

*Page 7, Line 29 and Line 32: Could you give a more quantitative description of land classes (in % or area size) for Table 1?*

8.1 Response to Referee: We have provided percent of observed footprints that fall into those land classes. In order to quantify based on land type, we more strictly followed the NSSI Landclass map; lakes and rivers have been combined to open water as they are according to NSSI.

8.2 Change to Manuscript: See imbedded table below.

Flight date DD.HH	Start time UTC - 10	End time UTC - 10	Temperature (°C)	Dominant land classes
25.18	17:43	19:49	5	Sedge (33%), Mesic sedge (19%), FWM (8%), Open Water (7%)
27.11	09:40	13:00	6	Open Water (31%), Sedge (26%), FWM (17%), Tussock Tundra (14%)
27.19	16:46	20:02	10	Sedge (44%), Open Water (16%) Mesic sedge (15%), FWM (15%)
28.10	08:39	11:39	11	Tussock tundra (46%), Open Water (26%), Sedge (19%), FWM (7%)
28.15	13:59	15:44	16	Sedge (47%), Mesic sedge (26%), FWM (8%), Open Water (7%)

#### 9. Referee 2 Comment

*Page 8: Line 27-30: Gene abundance does not directly refer to denitrification and N<sub>2</sub>O reduction rates. It still needs to be expressed so that N<sub>2</sub>O can be reduced. Better focus on the O<sub>2</sub> inhibition effect on N<sub>2</sub>O reductase.*

9.1 Response to Referee: Recognizing that gene abundance alone does not account for the fraction of the genes that are expressed in a population, the connection is at some level indicative of the population of the microbial community present. This argument is presented as one found in the literature that supports the possibility of N<sub>2</sub>O production instead of N<sub>2</sub> production. Here's the quote from the microbiology review paper we cite for that assertion:

“In the Arctic permafrost metagenomes that have been analysed so far, most of the genes that are involved in the denitrification pathway have been detected, but the relative gene abundances for the last steps in the pathway were too low to lead to N<sub>2</sub> production.”

The review then goes on to posit that a possible consequence of this is the accumulation of N<sub>2</sub>O. Because this is not our argument, but an argument from a published review paper in the field of microbiology, we will keep the sentence as is.

9.2 Change to Manuscript: None.

#### 10. Referee 2 Comment

*Abstract: Some explanation of the high N<sub>2</sub>O fluxes needs to be implemented. Also, please indicate the site location in the abstract.*

10.1 Response to Referee: We agree the site location should be in the abstract. We will add that along with the date. However, we feel that an explanation of the mechanism of the high N<sub>2</sub>O fluxes would be inappropriate since our results do not provide that insight, and explanations are largely based on insights provided by past chamber and laboratory studies. Having said that, we do provide more detail to our findings to clarify that our average represents observations with high variability.

10.2 Change to Manuscript: Page 1, Lines 15-17 has been altered as follows: “In late August 2013, we used the airborne eddy covariance technique to make *in situ* N<sub>2</sub>O flux measurements over the North Slope of Alaska from a low-flying aircraft spanning a much larger area: around 310 km<sup>2</sup>. We observed large variability of N<sub>2</sub>O fluxes with many areas exhibiting negligible emissions.”

# Permafrost Nitrous Oxide Emissions Observed on a Landscape Scale Using Airborne Eddy Covariance Method

Jordan Wilkerson<sup>1</sup>, Ronald Dobosy<sup>2,3</sup>, David S. Sayres<sup>4</sup>, Claire Healy<sup>5</sup>, Edward Dumas<sup>2,3</sup>, Bruce Baker<sup>2</sup>, and James G. Anderson<sup>1,4,5</sup>

<sup>1</sup>Department of Chemistry and Chemical Biology, Harvard University, Cambridge, MA 02138, USA; <sup>2</sup>Atmospheric Turbulence and Diffusion Division, NOAA/ARL, Oak Ridge, TN 37830, USA; <sup>3</sup>Oak Ridge Associated Universities (ORAU), Oak Ridge, TN 37830, USA; <sup>4</sup>Paulson School of Engineering and Applied Sciences, Harvard University, Cambridge, MA 02138, USA; <sup>5</sup>Department of Earth and Planetary Sciences, Harvard University, 12 Oxford Street, Cambridge, MA 02138, USA.

Correspondence to: Jordan Wilkerson (jwilkerson@g.harvard.edu)

**Abstract.** The microbial by-product nitrous oxide (N<sub>2</sub>O), a potent greenhouse gas and ozone depleting substance, has conventionally been assumed to have minimal emissions in permafrost regions. This assumption has been questioned by recent *in situ* studies demonstrating that, in fact, some geologic features in permafrost may have elevated emissions comparable to those of tropical soils. These recent studies, however, along with every known *in situ* study focused on permafrost N<sub>2</sub>O fluxes, have used chambers to examine small areas (< 50 m<sup>2</sup>). In late August 2013, we used the airborne eddy covariance technique, to make *in situ* N<sub>2</sub>O flux measurements over the North Slope of Alaska from a low-flying aircraft spanning a much larger area: around 310 km<sup>2</sup>. We observed large variability of N<sub>2</sub>O fluxes with many areas exhibiting negligible emissions. Still, the daily mean averaged over our flight campaign was 3.8 (2.2-4.7) mg N<sub>2</sub>O m<sup>-2</sup> d<sup>-1</sup> with 90% confidence interval in parentheses. If these measurements are representative of the whole month, then the permafrost areas we observed emitted a total of around 0.04-0.09 g m<sup>-2</sup> for August, comparable to what is typically assumed to be the upper limit of yearly emissions for these regions.

## 1 Introduction

N<sub>2</sub>O is the third most influential anthropogenic greenhouse gas behind CO<sub>2</sub> and CH<sub>4</sub>. Inert in the lowest atmospheric layer, N<sub>2</sub>O eventually rises into the stratosphere. There, photolysis and electronically excited oxygen atoms (O(<sup>1</sup>D)) convert N<sub>2</sub>O to nitrogen oxides that catalytically deplete ozone. N<sub>2</sub>O is currently the dominant ozone-depleting substance anthropogenically emitted. It is expected to remain so throughout the entire 21<sup>st</sup> century (Ravishankara et al. 2009). Due to increased industrial processes and agricultural practices that rely on heavy fertilization, N<sub>2</sub>O concentrations have been steadily rising in the atmosphere (Park et al. 2012). With a Global Temperature-change Potential over a 100-year time scale (GTP<sub>100</sub>) of 296, the climate system is more sensitive to changes in N<sub>2</sub>O concentrations than either of its carbon-based GHG counterparts (IPCC 2013).

While the global N<sub>2</sub>O budget can be divided into natural and anthropogenic sources, the two sectors have one thing in common: the primary mechanism of emission is denitrification by soil microbes (Syakila et al. 2011). For the anthropogenic sector, this primarily comes in the form of enhanced microbial activity in agricultural soils due to an imbalance between N fertilizer supply and crop uptake (Syakila et al. 2011). For the natural sector, tropical soils are considered the largest source of N<sub>2</sub>O (Zhuang et al. 2012). Meanwhile, N<sub>2</sub>O emissions from permafrost-laden regions have long been assumed to be negligible

Deleted: Using

Deleted: , we made

Deleted: a

Deleted: of

Deleted: maximum



(Martikainen et al. 1993; Potter et al. 1996) and are ignored in current N<sub>2</sub>O budgets (Zhuang et al. 2012; EPA 2010). This is largely because higher latitudes are considered nitrogen-limited and biogeochemically inactive relative to the tropics (Zhuang et al. 2012). However, recent *in situ* measurements of permafrost soils in [Russian tundra and northern Finland](#) (Repo et al. 2009; Marushchak et al. 2011) have found several geologic formations that may emit N<sub>2</sub>O fluxes comparable to tropical soil emissions (Zhuang et al. 2012). These formations include bare peat surfaces and thaw-induced permafrost collapse known as thermokarst. Elevated production of N<sub>2</sub>O in soil has also been observed in thermokarst features on the Alaskan North Slope (Abbott et al. 2015). All of these studies reported that these trends were sustained throughout the growing period. Furthermore, mesocosm studies in Finnish Lapland along with separate laboratory studies suggest that thawing permafrost further increases N<sub>2</sub>O production (Elberling et al. 2010; Voigt et al. 2017). Permafrost contains ~73 billion tons N in the upper 3 m of its soils (Harden et al. 2012). Considering this, better understanding the magnitude of current N<sub>2</sub>O emissions from Arctic surfaces is crucial given that the current rate of thaw is expected to continue or increase over the next century (Jones et al. 2016; Borge et al. 2017).

[The](#) past studies on permafrost N<sub>2</sub>O emissions have provided insight into the mechanisms of the gas's production and subsequent release into the atmosphere. [The studies](#) have been either laboratory studies or ground-based chamber studies. [In general, chamber studies have the advantage of observing the same site for relatively long time periods. Additional variables \(e.g. pH, water saturation\) can be monitored, too, which are crucial to understanding how that environment might influence the observed extent of N<sub>2</sub>O emissions. However, each chamber covers around 1 m<sup>2</sup>, and a feasible chamber study can only entail a limited number of sites. Consequently, past observations have covered extremely small areas – less than 50 m<sup>2</sup> \(Repo et al. 2009; Marushchak et al. 2011; Yang et al. 2018\). Therefore, the landscape scale of this phenomenon remains unknown, let alone the regional and continental scales. Landscapes deemed vulnerable to thaw-induced N<sub>2</sub>O emissions, permafrost and thermokarst regions, cover about one fourth of the Arctic/sub-Arctic \(Voigt et al. 2017\). One of those vulnerable areas is the Alaskan North Slope, which is the focus of this study. To get a landscape-scale estimate of the magnitude of permafrost N<sub>2</sub>O emissions during late summer, we measured N<sub>2</sub>O fluxes over the North Slope in late August 2013 using the airborne eddy covariance \(EC\) technique.](#)

EC technique has been applied to the trace gas nitrous oxide many times in the form of EC flux towers in regions other than permafrost. The first N<sub>2</sub>O EC flux tower measurements were published over a decade ago, using quantum cascade laser (QCL) spectroscopy (Kroon et al. 2007; Eugster et al. 2007). The specific QCL spectroscopic method used in this study to measure N<sub>2</sub>O mixing ratios, known as off-axis integrated cavity output spectroscopy (OA-ICOS), has also been applied to N<sub>2</sub>O EC flux measurements before (Zona et al. 2013). While the airborne EC technique has not previously been used to measure fluxes of the particular trace gas nitrous oxide, airborne EC has been used to measure trace gas fluxes at least over the past 30 years (Sellers et al. 1997). From multiple comparison studies, the airborne version of EC is considered as reliable as EC from a flux tower, the difference being that it averages over space instead of time (Mahrt et al. 1998; Gioli et al. 2004). The North Slope's large flat terrain makes it particularly suitable for airborne EC measurements (Hensen et al. 2013; Sayres et al. 2017).

## 2 Methods

[To evaluate landscape nitrous oxide fluxes in the North Slope, the Flux Observations of Carbon from an Airborne Laboratory \(FOCAL\) system \(shown in Fig. 1\) was flown out of Deadhorse Airport, Prudhoe Bay, AK. \(Note that while the system measured N<sub>2</sub>O flux, the name came from its ability to also measure CO<sub>2</sub> and CH<sub>4</sub> fluxes\). N<sub>2</sub>O measurements were made over five separate flights in several regions of the North Slope from 2013 August 25-28. The measurements entailed a cumulative path length of 884 km and approximate area coverage of 310 km<sup>2</sup> \(Fig. 2, Table 1\). Flights consisted of either repeated flight tracks near a CH<sub>4</sub>/H<sub>2</sub>O EC flux tower or 50 x 50 km grid patterns. In each flight, the flux calculations were restricted to straight segments flown below 50 m AGL. For the present study, segment sections over the open ocean were also excised.](#)

The low-flying aircraft flown in the campaign, a Diamond DA-42 from Aurora Flight Sciences, housed the two main components for flux measurements (Fig. 1): a turbulence probe and a custom-built IR spectrometer measuring water vapor,

Deleted: Russia

Deleted: While these

Deleted: , the observations

Deleted: at

Deleted: cover

Deleted: even

Deleted: ¶

Deleted: evaluate

Deleted: nitrous oxide fluxes in the North Slope, the Flux Observations...

Deleted: Carbon from an Airborne Laboratory (FOCAL) system (shown in Fig. 1) was flown in late August 2013 out

Deleted: Deadhorse Airport, Prudhoe Bay, AK. (Note that while the system measured

Deleted: flux, the name came from its ability to also measure CO<sub>2</sub> and CH<sub>4</sub> fluxes). We

Deleted: ~310 km<sup>2</sup> of

Deleted: with

CH<sub>4</sub>, and N<sub>2</sub>O at a rate of 10 times per second (10 Hz). These two components were used to measure the EC fluxes of N<sub>2</sub>O, CH<sub>4</sub>, and H<sub>2</sub>O during the 2013 campaign.

The flights near the flux tower were performed to compare the airborne CH<sub>4</sub> and H<sub>2</sub>O flux measurements with those from the EC flux tower (Dobosy et al. 2017). The CH<sub>4</sub> and H<sub>2</sub>O fluxes agreed with the ground measurement, and the CH<sub>4</sub> fluxes are consistent with other observed summertime permafrost CH<sub>4</sub> emissions reported in the scientific literature (Sayres et al. 2017). The only difference in the airborne flux measurements between CH<sub>4</sub>, H<sub>2</sub>O, and N<sub>2</sub>O is the particular absorption feature used within the observed spectral region of the IR instrument, as further discussed in Section 2.2 (Fig. 3).

## 2.1 BAT Probe Description and Calibration

The three wind components were measured using the Best Airborne Turbulence (BAT) probe developed by the National Oceanic and Atmospheric Administration/Atmospheric Turbulence and Diffusion Division (NOAA/ATDD) in collaboration with Airborne Research Australia (Crawford et al. 1993; Dobosy et al. 2013). The BAT probe also recorded ambient temperature and pressure measurements, which were used to determine dry air density. The aircraft was equipped with a radar altimeter, which in conjunction with three-component wind velocity measurements, was used for footprint calculations. These calculations were performed over 60 m segments along the flight track (Sayres et al. 2017). The footprints, representing the area from which the observed fluxes originated, were used to estimate the total area measured and identify which land classes were measured (Table 1).

The BAT probe, developed in the 1990s, is a type of gust probe consisting of a hemispherical head, 15.5 cm in diameter, with ports at selected positions on the hemisphere to sample the pressure distribution. A gust probe functions similarly to a typical pitot-static system but includes additional pressure measurements to sense the direction of the incoming flow along with its speed. The direction is specified in two perpendicular components called angles of attack and sideslip, which rarely exceed  $\pm 10^\circ$  in balanced flight (Leise et al. 2013). The BAT probe differs from other gust probes in having a larger head to accommodate accelerometers and pressure sensors directly in the head simplifying the physical and mathematical system needed to determine turbulent wind. It also has nine ports instead of the usual five found in traditional gust-probe systems. These additional four ports measure the ambient atmospheric pressure apart from small adjustments for nonzero attack and sideslip angles. Wind is sampled at 1000 Hz, filtered to control aliasing, and subsampled at 50 Hz.

The BAT probe configured for the FOCAL campaign (with the gas inlets in place) was characterized in a wind tunnel (Dobosy et al. 2013) following on an earlier wind-tunnel test of a similar unit in Indiana, USA (Garman et al. 2006). Its overall precision for wind is  $\pm 0.1 \text{ m s}^{-1}$ . With the entire instrument system assembled, standard-practice calibration maneuvers were flown in smooth air to establish the values of the tuning parameters for temperature, pressure, and wind measurement (Vellinga et al. 2013). Following the usual practice, we also made a calibration flight in smooth air on August 27 toward the end of the campaign (Sayres et al. 2017). Plots and comparison of spectra, cospectra, and time series for each flight provide tests of the quality of the data and of the processing through all intermediate steps.

## 2.2 N<sub>2</sub>O Instrument Description and Calibration

The gas inlet for the N<sub>2</sub>O instrument is located on the BAT probe housing, 8 cm aft of the probe's hemispherical face where ambient pressure and temperature measurements are made. The custom-built IR instrument uses Off-Axis Integrated Cavity Output Spectroscopy (OA-ICOS) to simultaneously measure H<sub>2</sub>O, CH<sub>4</sub>, and N<sub>2</sub>O (Fig. 4 & Fig. S1). The light source is a distributed feedback (DFB) continuous-wave quantum cascade laser (QCL) (Hamamatsu, LC0349). The laser tunes from 1292.5 to 1293.3  $\text{cm}^{-1}$  in 1.6 milliseconds. This region contains absorption features for H<sub>2</sub>O, CH<sub>4</sub>, and N<sub>2</sub>O (Fig. 3). Before the light enters the optical cavity, a beam-splitter diverts some of it through a Ge etalon. The etalon measures the rate at which the laser is tuning across the wavelength region, which is used to determine the width of the absorption lines. These components are all housed in the laser pressure vessel (Healy 2016).

The detection cell is a 25-cm length optical cavity composed of two high-reflectivity ZnSe mirrors (LohnStar Optics, R = 0.9996), which creates an effective path length of ~625 m. After leaving the cavity, the light enters the detector pressure vessel where it is focused onto a Stirling-cooled HgCdTe photoconductive detector (InfraRed Associates, Inc., MCT-12-2.05C). The detector system samples the light at 100 MHz and averages the readings to produce raw spectra with 1900 samples each. These spectra are then co-added to produce 1 spectrum every 0.1 sec and are stored on the flight computer.

Sample flow through the optical cavity is maintained in flight with a dry scroll pump that flushes the cell 17 times per second. The optical cavity is temperature and pressure-controlled to  $T = 303.70 \pm 0.05$  K and  $p = 59.26 \pm 0.01$  Torr, which allow conversion from concentration (moles  $\text{cm}^{-3}$ ) to mixing ratio (Webb et al. 1980, Gu et al. 2012). Cell temperature is measured by the average of two  $1 \text{ M}\Omega$  thermistors (General Electric, Type B) located within the cell, which were calibrated against a platinum primary standard. The cell is heated by polyimide thermofoil heaters, which are located along the cell exterior. The cell pressure is measured with a dual-headed absolute pressure transducer (MKS, D27D) and is controlled by a proportional solenoid valve. The valve is coupled with a pressure control board that uses the pressure transducer as feedback on the valve orifice's position (Fig. 1a) (Healy 2016).

$\text{H}_2\text{O}$  calibrations were performed using a dry-air tank coupled with a bubbler flow system as described in Weinstock et al. 2009. The  $\text{H}_2\text{O}$  measurements were used to account for dilution and water-broadening effects on the  $\text{N}_2\text{O}$  absorption feature and to convert the mixing ratio from moles per mole of total air to moles per mole of dry air for flux computation (Webb et al. 1980, Gu et al. 2012). The broadening coefficients were determined using the approach described in Rella 2010.

Periodic in-flight calibrations were performed to track and correct for drift over the course of the flight (2 calibration cycles per flight). These were performed using a secondary standard (277 ppbv  $\text{N}_2\text{O}$ ) calibrated in lab to a WMO standard (Sayres et al. 2017). Before and after the campaign, calibrations were also conducted in lab using two primary WMO standards and a synthetic air tank (containing no  $\text{N}_2\text{O}$ ) to calibrate the absorption coefficient and check for linearity. The short-term precision of the ICOS instrument for  $\text{N}_2\text{O}$  mixing ratios is determined using

$$\sigma = \sigma_{1s} f_s^{-1/2} \quad (1)$$

where  $\sigma_{1s}$  is the 1-second standard deviation for in-flight calibration data collected during that particular flight, and  $f_s$  is the sampling frequency in Hz (Kroon et al. 2007). Optical alignment was occasionally adjusted between flight days resulting in an  $\text{N}_2\text{O}$  precision range over the five flights of  $\sigma = 0.27\text{-}0.58$  ppb  $\text{Hz}^{1/2}$  (Table S1). This is close to the recommended precision for  $\text{N}_2\text{O}$  EC flux measurements as determined by previous studies evaluating the application of the EC technique to this particular trace gas; these groups also used QCL spectroscopy to measure  $\text{N}_2\text{O}$  mixing ratios (Kroon et al. 2007; Eugster et al. 2007).

### 2.3 Airborne EC Flux Calculations

The Airborne EC method relies on the fact that gases like  $\text{H}_2\text{O}$ ,  $\text{CH}_4$ , and  $\text{N}_2\text{O}$  emitted from the surface are transported upward into the atmospheric boundary layer by turbulent eddies. On average, upward flux occurs when updrafts are, more often than not, enriched in the transported gas relative to downdrafts. The covariance of vertical wind velocity with gas concentration is thus positive for upward flux, negative for downward.

To determine the covariance between vertical wind velocity  $w$  and  $\text{N}_2\text{O}$  mixing ratios  $c$ , we first separate each variable into changes associated with large-scale air motion (i.e. advection) and small-scale air motion (i.e. turbulence) (e.g.  $w = \bar{w} + w'$ ). We separated the two scales by fitting fourth-order polynomials to the measurements of  $w$  and  $c$  made along each individual straight leg of each flight (Fig. 2). The fit itself incorporates the larger scale trends (e.g.  $\bar{w}$ ), which are subtracted from the data. The remaining residuals from this fit are the turbulent quantities of interest (e.g.  $w'$ ) (Foken 2008).

Multiplying  $w$  by the density of dry air  $\rho_d$  and extracting the residual as discussed above, one obtains the turbulent dry air mass flux. The covariance of this dry-air flux  $(\rho_d w)'$  with the turbulent mixing ratio  $c'$  then yields the trace-gas flux of interest by the general EC approach (Webb et al. 1980, Gu et al. 2012):

$$F = \overline{(\rho_d w)'} c' \quad (2)$$

As previously mentioned, airborne EC measurements average over space instead of time. Accordingly, we compute the  $N_2O$  fluxes (along with  $CH_4$  and  $H_2O$  fluxes) using the [general](#) equation for airborne EC flux calculations:

Deleted: standard

$$F = \frac{\sum_{k=1}^N (\rho_d w)_k' c_k' V_k}{\sum_{k=1}^N V_k} \quad (3)$$

where  $V$  is the airspeed of the aircraft, and the other variables are defined as in Eq. (2) (Sayres et al. 2017; Dobosy et al. 2017). The true airspeed  $V = dl/dt$  is included in Eq. (3) to convert the variable of integration from time to space because the raw data are recorded at uniformly spaced time intervals (every 0.1 s) (Crawford et al. 1993). A number  $N$  of samples is being averaged, the denominator yielding their cumulative path length through the air.

Air density and vertical wind velocity  $w$  from the BAT probe are filtered and then subsampled at 10 Hz to match the measurement frequency for  $c_{N_2O}$ ,  $c_{CH_4}$ , and  $c_{H_2O}$ . Because the BAT probe observes a specific packet of air before the spectrometer does, a correction for the lag is applied to the data. The lag time from the gas inlet to the optical cavity was measured in the laboratory to be around 0.55 s. The lag between the BAT-probe measurements and those of the ICOS instrument in flight were determined by cross-correlation analysis of  $w$  and  $c_{CH_4}$ . They varied between 0.4 and 1.2 s. Methane was used as a proxy for  $N_2O$  to determine the lag because of its stronger signal.

Computation of dry air density uses the measured dry-air mixing ratio of  $H_2O$ . Turbulent quantities required for the footprint model are then computed by summing Eq. (3) over each flight segment. The mean  $N_2O$  fluxes displayed in Table 2 are computed by summing Eq. (3) over the multiple segments of each flight depicted in Fig. 2, excluding flight-path sections over coastal waters.

## 2.4 Flux Uncertainty Analysis

All confidence intervals reported in Table 2 and Table S1 are derived using bootstrap resampling (Dobosy et al. 2017), not from  $w$  and  $c_{N_2O}$  individually but from flux fragments (Sayres et al. 2017; Dobosy et al. 2017). These fragments are short (typically 1 s) blocks of integrated data that include the integrals of the three wind components, the height above ground, and the cross products of turbulent departure quantities from Eq. (3). All are integrated as above over the path through the air rather than time. They are each about 60 m long varying slightly due to small airspeed changes. These measurements, and therefore the corresponding confidence intervals, contain both environmental variability and variability arising from instrumental noise.

The fragments are serially correlated, and their means, trends, and variances are heterogeneous on scales greater than the 6 km found by ogive analysis to belong to turbulence. A procedure described by Mudelsee decomposes such partially determined, autocorrelated, and variably spaced data streams using the equation,

$$X(S) = T(S) + \sigma(S)R(S). \quad (4)$$

Here  $X(S)$  is a random-variable function over the path length  $S$  defined at irregular intervals (Mudelsee et al. 2010). The  $T(S)$  and  $\sigma(S)$  are the deterministic trend and variance of  $X(S)$  for each  $S$ , and  $R(S)$  is a serially correlated random-variable series having zero mean and unit variance. The  $T(S)$  and  $\sigma(S)$  for the current analysis are estimated as overlapping averages and variances of the measured fragments taken over 6 km, as determined by ogive analysis. They are evaluated at intervals of

1 km along the track and treated as fixed throughout the rest of the process. These larger scales can be treated as determinable from some (mesoscale) model.

The serial correlation of the random series  $R(S)$  is removed by a first-order Markov model, the inverse of a first-order causal filter (Dobosy et al. 2017). The resulting decorrelated series is (ideally) independent and “weakly” homogeneous (i.e., it has zero mean and unit variance). As such, it is suitable for bootstrap resampling. A resample size of 80,000 random decorrelated sequences, each the same length as the original set of fragments was drawn. The explained portion of the variance was then reapplied to each new resample using a process that is the reverse of the process of its removal, thus providing an ensemble of 80,000 new potential outcomes of the original experiment. The confidence intervals for  $N_2O$  flux were determined from the distribution of this population of reconstituted potential outcomes.

A Student’s  $t$ -test was also used to evaluate whether the Pearson’s correlation coefficient for  $w'$  and  $c_{N_2O}'$ , hence the  $N_2O$  flux, differs significantly from a random (zero) correlation (Eugster et al. 2015). Because the atmospheric data stream is serially correlated, as noted above, the  $N$  samples do not represent the total number of *independent* samples  $n$ . The number of independent samples is determined by:

$$n \cong N \frac{1-\rho_1}{1+\rho_1} \quad (5)$$

where  $\rho_1$  is the lag-1 autocorrelation coefficient (Eugster et al. 2015). The conclusions of this test are folded into Table 2 in the Results and Discussion section.

## 2.5 Footprint and Land Class Determination

Following Sayres et al. 2017, the model developed by Kljun et al. 2004 is used to derive a footprint for each 60-m flux fragment. The wind and height above ground level are averaged over the fragment, and the required turbulence quantities are averaged over the flight leg containing the fragment. This procedure accounts for variations in mean wind and height above ground along the track while using the longer average required for flux computation. The footprints are used to estimate each flux fragment’s related source area on the surface. The set union of these source areas constitutes the total area covered by each flight. Each flux fragment’s coverage area is estimated by multiplying the length accounting for 90% of the crosswind-integrated probability in the footprint by the path length of the respective flux fragment. For Flights 25.18 and 27.19, the aircraft sometimes flies over the same path multiple times during the same flight. In these cases, the observed area is only counted once. These areas are summed for all of the fragments in each flight (Table 2).

For determining the land classes associated with the flux footprints, we use a land cover map developed by the North Slope Science Initiative (NSSI). There were 24 land classes used for the NSSI classification scheme (NSSI 2013). However, for our land classification, the following land classes are conflated: Tussock Tundra and Tussock Shrub Tundra; Freshwater Marsh Arctophila Fulva and Freshwater Marsh Carex Aquatilis; Dwarf Shrub – Dryas and Dwarf Shrub – Other; Ice/Snow and Open Water.

## 3 Results

### 3.1 Cospectra and Ogives

A cospectrum, the spectral decomposition of the covariance of the vertical wind velocity and trace gas mixing ratio, reveals the contribution to the overall flux from turbulent eddies as a function of their size. Starting from the smallest scales, the cospectrum normally increases to a maximum and then returns to near zero, sometimes increasing again at still larger scales. The cumulative integral of the cospectrum up to its first return to zero is known as the ogive. The cospectra and ogives averaged over the entire campaign are shown for  $H_2O$ ,  $CH_4$ , and  $N_2O$  in Fig. 5.

The usual cospectrum has the shape of the H<sub>2</sub>O flux (blue). This cospectrum reaches a peak around 300 m above which the incremental contribution to the flux declines with increasing eddy scale reaching near zero in this case at about 6 km. This length is taken to be the largest scale of boundary-layer turbulence for H<sub>2</sub>O. It is, therefore, the minimum averaging length for H<sub>2</sub>O fluxes. For the ogive, this point corresponds to the inflection point (zero slope). The cospectrum and ogive curves are normalized by the value of the ogive at its inflection point. The ogive thus reaches unity at its inflection point, where it is proportional to the mean flux density ( $\text{g m}^{-2} \text{s}^{-1}$ ) of H<sub>2</sub>O.

The cospectra of the remaining two gases (CH<sub>4</sub> & N<sub>2</sub>O) follow the same pattern but with considerably more scatter due to the weaker flux of these gases, among other things. The ogive of N<sub>2</sub>O in particular shows notably strong contributions from the smaller scales (below 80 m) and the larger scales (above 500 m) perhaps resulting from a spotty distribution of sources (e.g., Fig. 6). The maximum turbulent scales for CH<sub>4</sub> and N<sub>2</sub>O were taken from these ogives to be 4 km and 6 km, respectively.

### 3.2 Spatial Distribution of N<sub>2</sub>O Flux

Fig. 6 shows a spatial map of N<sub>2</sub>O emissions measured during Flight 28.10. The individual points represent running averages obtained by summing Eq. (3) over 6 km paths with 3 km overlap. The choice of 6-km averaging length for Flight 28.10 was determined by ogive analysis as discussed above (Foken 2008).

The detection limit for observing these 6-km average N<sub>2</sub>O fluxes was estimated by computing the running averages using Eq. (3) as described above but replacing the measured environmental  $c_{\text{N}_2\text{O}}$  with a synthetic vector of the same length (~55 min.). The synthetic vector was assembled by random resampling with replacement from 3 minutes (1800 samples) of N<sub>2</sub>O mixing ratio obtained during the same flight from a cylinder having known N<sub>2</sub>O mixing ratio. All other data streams, such as  $\rho_a$  and  $w$ , containing both instrumental and environmental variability, remained unchanged. These 6-km running averages composed of calibration data had mean  $0.0 \pm 0.05 \mu\text{g N}_2\text{O m}^{-2} \text{s}^{-1}$  (standard deviation). We use  $2\sigma$  to define the instrumental uncertainty of the 6-km averages and treat 6-km average values between  $\pm 0.1 \mu\text{g N}_2\text{O m}^{-2} \text{s}^{-1}$  in Fig. 6 as indistinguishable from zero.

While Flight 28.10 had a significant overall average emission (Table 2), Fig. 6 illustrates that much of that emission arises in multiple small-scale domains (commonly referred to as ‘hot spots’) with approximately half of the 6-km means being indistinguishable from zero given the instrumental uncertainty described above. This hot-spot pattern is true for the other flights as well. This highlights the spatiotemporal variability characteristic of soil N<sub>2</sub>O emissions and could help explain why permafrost N<sub>2</sub>O emissions studies, which are sparse and rely on extremely small spatial sampling when done, often detect no significant flux (Kroon et al. 2007; Butterbach-Bahl et al. 2013).

### 3.3 N<sub>2</sub>O Flux Averages

The whole-flight spatially averaged N<sub>2</sub>O fluxes for each flight and the approximate surface area covered are shown in Table 2. Several of the averages are higher than have been assumed for N<sub>2</sub>O emissions at these latitudes. For example, the average N<sub>2</sub>O flux from tundra is considered to be around  $0.005 \mu\text{g N}_2\text{O m}^{-2} \text{s}^{-1}$  (Potter et al. 1996). By contrast, the whole-flight average from Flight 28.10, dominantly from tussock tundra (Table 1), was  $0.104 \mu\text{g N}_2\text{O m}^{-2} \text{s}^{-1}$ , 20 times higher than the assumed value. Of the five flights, there are two flights where the average agrees with the expectation of negligible emissions (Flights 27.11 and 27.19). The flight where we observed the lowest average N<sub>2</sub>O flux, Flight 27.11, covered land surfaces significantly more waterlogged than the other flights (Table 1). This observation is consistent with the established understanding that water saturation acts as a suppressant of nitrous oxide emissions because N<sub>2</sub>O is instead anaerobically processed into N<sub>2</sub> by nitrous oxide reductase, an enzyme hypothesized to be inhibited by O<sub>2</sub> (Morley et al. 2008; Butterbach-Bahl et al. 2013).

Explaining the low mean flux for Flight 27.19 is less straightforward. Even though the path of Flight 27.19 was in the same proximity as Flights 25.18 and 28.15, Flight 27.19 has a noticeably lower average than the other two, which have similar mean fluxes (Table 2). Because this was an evening flight under reduced solar radiation, the boundary layer may have been too shallow to communicate the full emission of N<sub>2</sub>O from the surface to the flight level where it could be measured (Sayres et al.

2017). Separately, Table 1 shows that the ordering of the land classes measured was the same for all three flights. However, Flight 27.19's contribution from lakes and freshwater marsh was higher than from the other flights in that area (Sayres et al. 2017). Therefore, the comparatively lower average could also be a consequence of that flight's footprints covering a higher fraction of waterlogged environments.

The mean flux for all flights is  $0.043 \mu\text{g N}_2\text{O m}^{-2} \text{s}^{-1}$  (Table 2). This average is significantly different from zero flux ( $p < 0.01$ ) as determined by both bootstrap-derived CIs and the student's  $t$ -test as described in the Methods section (see Table S1 for 99% CI ranges). This corresponds to a daily mean between  $2.2\text{--}4.7 \text{ mg N}_2\text{O m}^{-2} \text{d}^{-1}$  (this range represents the 90% CI values in Table 2 being converted to  $\text{mg N}_2\text{O m}^{-2} \text{d}^{-1}$ ). These observed  $\text{N}_2\text{O}$  emissions are higher than expected (Zhuang et al. 2012). However, there have been several small-scale chamber studies that have observed  $\text{N}_2\text{O}$  emissions within this mean daily range (Repo et al. 2009; Marushchak et al. 2011; Yang et al. 2018). Soil analyses on the North Slope thermokarst features in upland tundra have also found elevated soil  $\text{N}_2\text{O}$  concentrations sustained throughout the growing season (Abbott et al. 2015). These elevated levels were attributed to abrupt thaw processes known as thermokarst, which can cause permafrost to collapse. This displaced soil redistributes soil organic matter into both oxic and anoxic environments, a condition conducive to producing  $\text{N}_2\text{O}$  as a final product instead of as a metabolic intermediate for  $\text{N}_2$  (Abbott et al. 2015). Transitions, in general, from oxic to anoxic environments (and vice versa) are well-known to induce spikes in  $\text{N}_2\text{O}$  emissions for a variety of soils (Schreiber 2012).

If results from the last week of August are representative of the whole month, the  $\text{N}_2\text{O}$  emission over the span of August is  $\sim 0.04\text{--}0.09 \text{ g N m}^{-2}$ . This range contains what is currently assumed to be the maximum emission over an entire year at these latitudes ( $\sim 0.05 \text{ g N m}^{-2} \text{yr}^{-1}$ ) (EPA 2010; Zhuang et al. 2012). Past static chamber studies and soil studies that measured elevated permafrost  $\text{N}_2\text{O}$  production observed that it was sustained throughout the entire growing period, which spans several months. One of these studies (Abbott et al. 2015) specifically examined permafrost in the North Slope, same as in our campaign. Furthermore, these studies largely attribute the elevated rate of soil  $\text{N}_2\text{O}$  production to higher soil temperatures (Repo et al. 2009; Abbott et al. 2015). Soil temperatures taken near our flux tower were lower during our observation period than in previous weeks of August 2013 (Fig. S2).

#### 4 Discussion

A body of evidence suggests the nutrient composition of, and microbial communities within, permafrost soils can be conducive to nitrous oxide production. Boreal peat soils are known to have negligible  $\text{N}_2\text{O}$  emissions when soil C/N ratios are above 25 (Klemmedtsson et al. 2005). However, below this threshold,  $\text{N}_2\text{O}$  fluxes can increase quite rapidly with decreasing C/N ratios. For the upper 3 m of permafrost, all three subsets of permafrost soils (histel, turbel, and orthel) have mean C/N ratios below 25, with turbel soils averaging the lowest at  $\sim 15$  (Harden et al. 2012). Importantly, these values are averaged over many studies; the C/N ratio is highly variable. For example, eight yedoma (organic-rich permafrost soil) and thermokarst sites in Arctic Siberia were reported to have C/N ratios of 11, averaged over 3 m depth (Fuchs et al. 2017). To reiterate, the upper 3 m is relevant for permafrost collapse, which routinely exposes deeper soil to the atmosphere. Not only are these C/N ratios suitable for  $\text{N}_2\text{O}$  production, metagenomic analyses (analyses quantifying relative abundance of genes in an environmental sample) performed on permafrost cores suggest  $\text{N}_2\text{O}$  is likely the final product for denitrification. This is because while most of the genes for the denitrification pathway were observed, the relative abundance of genes corresponding to the final steps was too low to lead to any significant conversion of  $\text{N}_2\text{O}$  to  $\text{N}_2$  (Jansson et al. 2014).

It is unclear whether these observed emissions signify a recent trend or have been constant over time because the data collected on permafrost  $\text{N}_2\text{O}$  fluxes are severely limited. No estimate of permafrost  $\text{N}_2\text{O}$  emissions before the Industrial Revolution exists, and few data have been collected since (Davidson et al. 2014). Therefore, it is unknown how these emissions have changed since global climate change started significantly affecting the permafrost landscape. However, it is well established that the troposphere at these higher latitudes has warmed, on average, 1.9 times more than the global average (Serreze et al. 2011). Soil temperatures have increased as well. Temperatures of permafrost soils in Northern Alaska, for example, increased by up to  $3^\circ\text{C}$  since the 1980s (IPCC 2013). Permafrost warming/thaw, independent of permafrost collapse, has been demonstrated to increase  $\text{N}_2\text{O}$  emissions significantly (Elberling et al. 2010; Voigt et al. 2016; Voigt et al. 2017).

Furthermore, this temperature increase has induced permafrost degradation over time, which has manifested as the expansion of thermokarst features shown to promote elevated N<sub>2</sub>O production even further as discussed above. Finally, increased permafrost thaw may make soil drainage more efficient, thus reducing the extent of waterlogged environments in higher latitudes (Avis et al. 2011). More streamlined draining also allows for a greater extent of draining and rewetting of permafrost soils, a process shown to increase thawed permafrost emissions of N<sub>2</sub>O ten-fold (Elberling et al. 2010). All of the observed changes to permafrost discussed above are variables that have been examined with respect to nitrous oxide emissions, and they have all have been shown to increase the fluxes of this gas. Based on this existing literature, our observed N<sub>2</sub>O emissions may reflect a positive climate feedback already in progress. That being said, it is unclear to what extent future emission rates will increase because soil temperature is only one of many factors that will continue to change at high latitudes, with increasing vegetation being the most likely to negate the effects of increasing soil temperatures (Repo et al. 2009; Voigt et al. 2017).

## 5 Conclusion

In this campaign, we flew over ~310 km<sup>2</sup> of the Alaskan North Slope and measured N<sub>2</sub>O flux using the airborne Eddy Covariance technique. We observed spotty spatial distribution of elevated N<sub>2</sub>O emissions that averaged to 0.043 (0.025, 0.055) µg N<sub>2</sub>O m<sup>-2</sup> s<sup>-1</sup>. These results corroborate several recent studies that used the static chamber method and observed permafrost soils emitting significant levels of nitrous oxide that are sustained throughout the entire growing period. This is a contrast to the traditional view regarding emissions at these latitudes. Importantly, we corroborate these findings in a complementary way: by observing fluxes on a landscape scale rather than the much smaller-scale soil plots in chamber studies, [which are intended more to understand temporal representativeness and mechanisms of N<sub>2</sub>O production](#). While our study spans a spatial coverage greater by orders of magnitude than any previous study, it is still preliminary because the Arctic/sub-Arctic covers a vast area. This limitation notwithstanding, we demonstrate that it is possible to apply the established airborne EC technique to the trace gas nitrous oxide to more thoroughly evaluate emissions of N<sub>2</sub>O in permafrost regions. This approach is a useful supplement since most of the landscape is remote and inhospitable, making maintenance of flux towers and chambers intractable.

Climate projection models and stratospheric ozone depletion assessments rely on global N<sub>2</sub>O budgets to predict future atmospheric scenarios (Ravishankara et al. 2009; Meinshausen et al. 2011). Considering the observed N<sub>2</sub>O fluxes reported here, more field campaigns that employ airborne EC technique or similar measurement techniques designed for much larger spatial coverage should be employed. These should also be coupled with ground-based measurements that can help corroborate airborne findings and better pinpoint where elevated N<sub>2</sub>O emissions might be occurring. Campaigns like these would help better determine whether the current, data-limited assumption of negligible N<sub>2</sub>O emissions is a correct one. If permafrost N<sub>2</sub>O emissions are already not negligible, their predicted increase with warming permafrost soil temperatures could result in a noncarbon climate feedback of a currently unanticipated magnitude.

**Data Availability.** The datasets generated and analyzed during the current study are available at: Sayres, D., Dobosy, R. Alaska 2013 Campaign. *Harvard Dataverse*, V1. doi: 10.7910/DVN/YM70Y7 (2018).

## Author contributions

B.B., R.D., D.S.S., and J.G.A. designed the study. D.S.S., E.D., and C.H. contributed to instrument development, data collection and field work. J.W. and R.D. contributed to data processing and uncertainty analysis. J.W. was mainly responsible for interpreting the results and writing the manuscript. All authors participated in writing/editing the manuscript.

## Competing interests

The authors declare that they have no conflict of interest.



## Acknowledgements

We thank M. Rivero, N. Allen, and C. Tuozzolo for their laboratory and field assistance; Bernard Charlemagne for piloting the aircraft; J.B. Smith, E. Moisson, and A. Bendelsmith for their comments on the manuscript. This work was funded by NSF grant 1203583.

## References

Abbott, B. W. & Jones, J. B.: Permafrost collapse alters soil carbon stocks, respiration, CH<sub>4</sub>, and N<sub>2</sub>O in upland tundra, *Glob Change Biol*, 21, 4570–4587, <https://doi.org/10.1111/gcb.13069>, 2015.

Avis, C. A., Weaver, A. J. & Meissner, K. J.: Reduction in areal extent of high-latitude wetlands in response to permafrost thaw. *Nature Geosci*, 4, 444–448, <https://doi.org/10.1038/ngeo1160>, 2011.

Borge, A. F., Westermann, S., Solheim, I. & Etzelmüller, B.: Strong degradation of palsas and peat plateaus in northern Norway during the last 60 years. *The Cryosphere*, 11, 1–16, <https://doi.org/10.5194/tc-11-1-2017>, 2017.

Butterbach-Bahl, K., Baggs, E. M., Dannenmann, M., Kiese, R. & Zechmeister-Boltenstern, S.: Nitrous oxide emissions from soils: how well do we understand the processes and their controls? *Philosophical Transactions of the Royal Society B: Biological Sciences*, 368, 20130122–20130122, <https://doi.org/10.1098/rstb.2013.0122>, 2013.

Crawford, T., McMillen R., Dobosy, R., & MacPherson, I.: Correcting airborne flux measurements for aircraft speed variation. *Boundary-Layer Meteorology*, 66, 237–245, 1993.

Davidson, E. A. & Kanter, D.: Inventories and scenarios of nitrous oxide emissions. *Environ. Res. Lett.*, 9, 105012–13, 2014.

Dobosy, R. et al.: Calibration and Quality Assurance of an Airborne Turbulence Probe in an Aeronautical Wind Tunnel. *J. Atmos. Oceanic Technol.*, 30, 182–196, <https://doi.org/10.1175/JTECH-D-11-00206.1>, 2013.

Dobosy, R., et al.: Estimating random uncertainty in airborne flux measurements over Alaskan tundra: Update in the Flux-Fragment Method. *J. Atmos. Oceanic Technol.*, 34, 1807–1822, <https://doi.org/10.1175/JTECH-D-16-0187.1>, 2017.

- Elberling, B., Christiansen, H. H. & Hansen, B. U.: High nitrous oxide production from thawing permafrost. *Nature Geosci.*, 3, 332–335, <https://doi.org/10.1038/ngeo893>, 2010.
- Eugster, W., et al.: Methodical study of nitrous oxide eddy covariance measurements using quantum cascade laser spectrometry over a Swiss forest. *Biogeosciences*, 4, 927–939, <https://doi.org/10.5194/bg-4-927-2007>, 2007.
- Eugster, W. and Merbold, L.: Eddy covariance for quantifying trace gas fluxes from soils. *Soil*, 1, 187–205, <https://doi.org/10.5194/soil-1-187-2015>, 2015.
- Foken, T. *Micrometeorology*. 2<sup>nd</sup> ed. 113–115 (Bayreuth, Germany: Springer-Verlag, 2008).
- Fuchs, M. et al.: Carbon and nitrogen pools in thermokarst-affected permafrost landscapes in Arctic Siberia. *Biogeosciences Discuss.*, 1–35, <https://doi.org/10.5194/bg-15-953-2018>, 2017.
- Garman, K., et al.: An airborne and wind tunnel evaluation of a wind turbulence measurement system for aircraft-based flux measurements. *Journal of Atmospheric and Oceanic Technology*, 23, 1696–1708, <https://doi.org/10.1175/JTECH1940>, 2006.
- Gioli, B., et al.: Comparison between tower and aircraft-based eddy covariance fluxes in five European regions. *Agricultural and Forest Meteorology*, 127, 1–16, <https://doi.org/10.1016/j.agrformet.2004.08.004>, 2004.
- Gu, L., Massman, W.J., Leuning, R., Pallardy, S.G., Meyers, T., Hanson, P.J., Riggs, J.S., Hosman, K.P. and Yang, B.: The fundamental equation of eddy covariance and its application in flux measurements. *Agricultural and Forest Meteorology*, 152, 135–148, <https://doi.org/10.1016/j.agrformet.2011.09.014>, 2012.
- Harden, J. W. et al.: Field information links permafrost carbon to physical vulnerabilities of thawing. *Geophys. Res. Lett.*, 39, 71–6, <https://doi.org/10.1029/2012GL051958>, 2012.
- Healy, C.: Mapping and Characterizing the Alaskan North Slope Methane Flux With Airborne Eddy-Covariance Flux Measurements. Doctoral dissertation, Harvard University, Graduate School of Arts & Sciences, 2016.
- Hensen, A., Skiba, U. & Famulari, D.: Low cost and state of the art methods to measure nitrous oxide emissions. *Environ. Res. Lett.*, 8, 025022–11, <https://doi.org/10.1088/1748-9326/8/2/025022>, 2013.

- Intergovernmental Panel on Climate Change (IPCC).in Climate Change 2013: The Physical Science Basis (eds. Stocker, T et al.) (Cambridge Univ. Press, 2013).
- Jansson, J. K. & Taş, N.: The microbial ecology of permafrost. *Nature Reviews Microbiology*, 12, 414–425, <https://doi.org/10.1038/nrmicro3262>, 2014.
- Jones, B. M. et al.: Presence of rapidly degrading permafrost plateaus in south-central Alaska. *The Cryosphere*, 10, 2673–2692, <https://doi.org/10.5194/tc-10-2673-2016>, 2016.
- Klemetsson, L., Arnold, Von, K., Weslien, P. & Gundersen, P.: Soil CN ratio as a scalar parameter to predict nitrous oxide emissions. *Glob Change Biol*, 11, 1142–1147, <https://doi.org/10.1111/j.1365-2486.2005.00973.x>, 2005.
- Kljun, N., Calanca, P., Rotach, M., & Schmid, H.: A simple parameterization for flux footprint predictions. *Boundary-Layer Meteorology*, 112, 503–523, <https://doi.org/10.1023/B:BOUN.0000030653.71031.96>, 2004.
- Kroon, P. et al.: Suitability of quantum cascade laser spectroscopy for CH<sub>4</sub> and N<sub>2</sub>O eddy covariance flux measurements. *Biogeosciences*, 4, 715–728, <https://doi.org/10.5194/bg-4-715-2007>, 2007.
- Leise, J. A., J. M. Masters, and R. J. Dobosy. National Oceanic and Atmospheric Association. Wind measurements from aircraft. NOAA Tech. Memo.OAR-266, 209, <https://doi.org/10.7289/V5/TM-OAR-ARL-266>, 2013.
- Mahrt, L.: Flux Sampling Errors for Aircraft and Towers. *Journal of Atmospheric and Ocean Technology*, 15, 416–428, [https://doi.org/10.1175/1520-0426\(1998\)015<0416:FSEFAA>2.0.CO;2](https://doi.org/10.1175/1520-0426(1998)015<0416:FSEFAA>2.0.CO;2), 1998.
- Martikainen, P. J., Nykänen, H., Crill, P. & Silvola, J.: Effect of a lowered water table on nitrous oxide fluxes from northern peatlands. *Nature*, 366, 51–53, 1993.
- Marushchak, M. E. et al.: Hot spots for nitrous oxide emissions found in different types of permafrost peatlands. *Glob Change Biol* 17, 2601–2614, <https://doi.org/10.1111/j.1365-2486.2011.02442.x>, 2011.
- Meinshausen, M. et al.: The RCP greenhouse gas concentrations and their extensions from 1765 to 2300. *Climatic Change*, 109, 213–241, <https://doi.org/10.1007/s10584-011-0156-z>, 2011.

- Morley, N., Baggs, E. M., Dörsch, P., & Bakken, L.: Production of NO, N<sub>2</sub>O and N<sub>2</sub> by extracted soil bacteria, regulation by NO<sub>2</sub><sup>-</sup> and O<sub>2</sub> concentrations. *FEMS Microbiology Ecology*, 65, 102–112, <https://doi.org/10.1111/j.1574-6941.2008.00495.x>, 2008.
- 5 Mudelsee, M. *Climate Time Series Analysis: Classical Statistical and Bootstrap Methods*. 2<sup>nd</sup> ed. p 474 (Cham, Switzerland: Springer, 2010).
- North Slope Science Initiative: North Slope Science Initiative Landcover Mapping Summary Report, 2013. Available at: <http://catalog.northslopescience.org/catalog/entries/4616-nssi-landcover-report-landcover-mapping-for-north-slope-of-alaska>  
 10 (last accessed: 27 January 2018).
- Park, S. et al.: Trends and seasonal cycles in the isotopic composition of nitrous oxide since 1940. *Nature Geosci*, 5, 261–265, <https://doi.org/10.1038/ngeo1421>, 2012.
- 15 Potter, C., Matson, P., Vitousek, P., & Davidson, E.: Process modeling of controls on nitrogen trace gas emissions from soils worldwide. *Journal of Geophysical Research*, 101, 1361–1377, <https://doi.org/10.1029/95JD02028>, 1996.
- Ravishankara, A. R., Daniel, J. S. & Portmann, R. W.: Nitrous Oxide (N<sub>2</sub>O): The Dominant Ozone-Depleting Substance Emitted in the 21st Century. *Science* 326, 123–125, <https://doi.org/10.1126/science.1176985>, 2009.
- 20 Rella, C.: Accurate Greenhouse Gas Measurements in Humid Gas Streams Using the Picarro G1301 Carbon Dioxide/Methane/Water Vapor Gas Analyzer. Picarro, Inc, 2010.
- Repo, M. E. et al.: Large N<sub>2</sub>O emissions from cryoturbated peat soil in tundra. *Nature Geosci*, 2, 189–192,  
 25 <https://doi.org/10.1038/ngeo434>, 2009.
- Sayres, D. S. et al.: Arctic regional methane fluxes by ecotope as derived using eddy covariance from a low-flying aircraft. *Atmos. Chem. Phys.*, 17, 8619–8633, <https://doi.org/10.5194/acp-17-8619-2017>, 2017.
- 30 Schreiber, F., Wunderlin, P., Udert, K.M., Wells, G.F.: Nitric oxide and nitrous oxide turnover in natural and engineered microbial communities: biological pathways, chemical reactions, and novel technologies. *frontiers in Microbiology*, 3, 1–24, <https://doi.org/10.3389/fmicb.2012.00372>, 2012.

- Sellers, P. et al.: BOREAS in 1997: Experiment overview, scientific results, and future directions. *Journal of Geophysical Research* 102, 28731-69, <https://doi.org/10.1029/97JD03300>, 1997.
- Serreze, M. C. & Barry, R. G.: Processes and impacts of Arctic amplification: A research synthesis. *Global and Planetary Change*, 77, 85–96, <https://doi.org/10.1016/j.gloplacha.2011.03.004>, 2011.
- Syakila, A. & Kroeze, C.: The global nitrous oxide budget revisited. *Greenhouse Gas Measurement and Management*, 1, 17–26, <https://doi.org/10.3763/ghgmm.2010.0007>, 2011.
- 10 United States Environmental Protection Agency. (2010) Methane and Nitrous Oxide Emissions From Natural Sources.
- Vellinga, O., et al.: Calibration and quality assurance of flux observations from a small research aircraft. *J. Atmos. Oceanic Technol.*, 30, 161-181, <https://doi.org/10.1175/JTECH-D-11-00138.1>, 2013.
- 15 Voigt, C. et al.: Warming of subarctic tundra increases emissions of all three important greenhouse gases - carbon dioxide, methane, and nitrous oxide. *Glob Change Biol*, 23, 3121–3138, <https://doi.org/10.1111/gcb.13563>, 2016.
- Voigt, C. et al.: Increased nitrous oxide emissions from Arctic peatlands after permafrost thaw. *Proc Natl Acad Sci USA*, 114, 6238–6243, <https://doi.org/10.1073/pnas.1702902114>, 2017.
- 20 Webb, E., Pearman, G., & Leuning, R.: Correction of flux measurements for density effects due to heat and water vapour transfer. *Quart. J. R. Met. Soc.*, 106, 85-100, <https://doi.org/10.1002/qj.49710644707>, 1980.
- 25 Weinstock, E., et al.: Validation of the Harvard Lyman-  $\alpha$  in situ water vapor instrument: Implications for the mechanism that control stratospheric water vapor. *J. Geophys. Res.*, 114, D23301, <https://doi.org/10.1029/2009JD012427>, 2009.
- Yang, G. et al.: Magnitude and Pathways of Increased Nitrous Oxide Emissions from Uplands, Following Permafrost Thaw. *Environmental Science & Technology*, 52, 9162-9169, <https://doi.org/10.1021/acs.est.8b02271>, 2018.
- 30 Zhuang, Q., Lu, Y. & Chen, M.: An inventory of global N<sub>2</sub>O emissions from the soils of natural terrestrial ecosystems. *Atmospheric Environment*, 47, 66–75, 2012.

Zona, D., et al.: Fluxes of the greenhouse gases (CO<sub>2</sub>, CH<sub>4</sub> and N<sub>2</sub>O) above a short-rotation poplar plantation after conversion from agricultural land. *Agricultural and Forest Meteorology*, 164, 100-110, <https://doi.org/10.1016/j.agrformet.2012.10.008>, 2013.

Figures and Tables

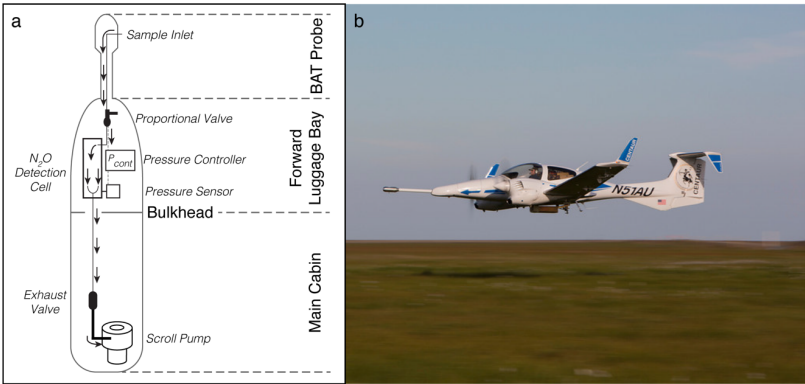


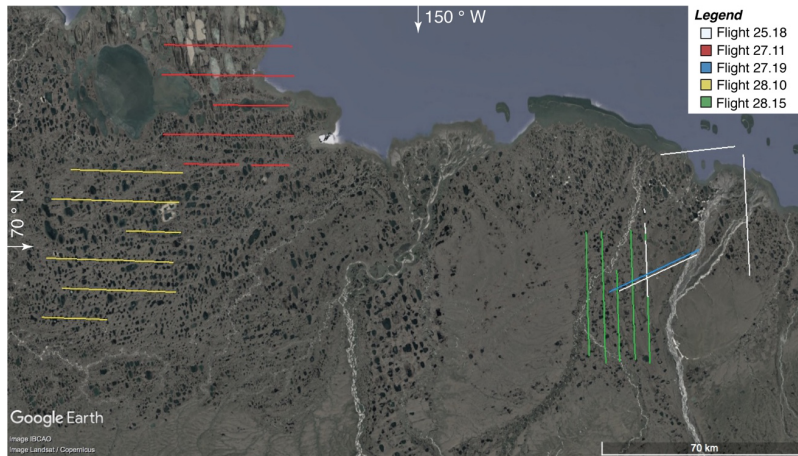
**Figure 1.** FOCAL during flight. **a**, Top-down schematic of the atmospheric gas flow through the aircraft (not to scale). The sample inlet is located on the BAT probe, located at the nose of the plane. The gas is pumped through the pressure-regulated detection cell of the ICOS spectrometer, located within the luggage bay in front of the pilot. **b**, Image of the Diamond DA-42 flying around 15 m above the surface.

5

10

15

20

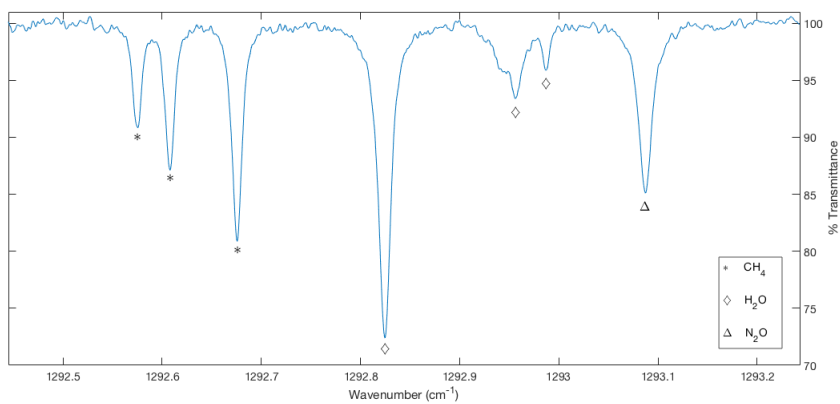


25 **Figure 2.** Flight tracks for August 2013 campaign where the paths represent sections of the flights that were suitable for flux calculations (aircraft flying on a straight, level path below 50 m). (Map image credit: Google Earth).

30

5

10



15 **Figure 3.** Sample 10-Hz ICOS spectrum taken from Flight 28.10.

20



5

10

15 **Table 1. Description of August 2013 Flights.** Flight date is the day of the flight in August (DD) and middle time of flight to nearest hour (HH). Temperature is the air temperature measured during the flight, averaged over all measurements made below 100 m. The dominant land classes are listed in order of decreasing relative contribution to the observed fluxes, determined by footprint analysis coupled with a landcover map. (FWM, Fresh Water Marsh).

Flight date	Start time	End time	Temperature	Dominant land classes
DD,HH	UTC - 10	UTC - 10	(°C)	
25 18	17:43	19:49	5	Sedge, (33%), Mesic sedge, (19%), FWM (8%), Open Water (7%)
27 11	09:40	13:00	6	Open Water (31%), Sedge, (26%), FWM, (17%), Tussock Tundra (14%)
27 19	16:46	20:02	10	Sedge, (44%), Open Water (16%), Mesic sedge, (15%), FWM (15%)
28 10	08:39	11:39	11	Tussock tundra, (46%), Open Water (26%), Sedge, (19%), FWM (7%)
28 15	13:59	15:44	16	Sedge, (47%), Mesic sedge, (26%), FWM (8%), Open Water (7%)

20

Formatted: Font: 8.5 pt

Formatted: Font: 8.5 pt

Deleted: ,

Formatted: Font: 8.5 pt

Deleted: , Lakes, Sag River,

Formatted: Font: 8.5 pt

Formatted: Font: 8.5 pt

Formatted: Font: 8.5 pt

Formatted: Font: 8.5 pt

Deleted: ,

Formatted: Font: 8.5 pt

Deleted: , Lakes,

Formatted: Font: 8.5 pt

Formatted: Font: 8.5 pt

Deleted: , Lakes, Sag River,

Formatted: Font: 8.5 pt

Formatted: Font: 8.5 pt

Formatted: Font: 8.5 pt

Formatted: Font: 8.5 pt

Deleted: , Lakes,

Formatted: Font: 8.5 pt

Deleted: ,

Formatted: Font: 8.5 pt

Formatted: Font: 8.5 pt

Formatted: Font: 8.5 pt

Deleted: ,

Formatted: Font: 8.5 pt

Deleted: , Lakes, Kuparuk River,

Formatted: Font: 8.5 pt

Formatted: Font: 8.5 pt

5

10

**Table 2: Observed flux averages.** Area covered is the footprint scope of the measurements made for each flight. Spatially averaged fluxes are presented with bootstrap-derived 90% confidence intervals in parentheses. Asterisks indicate mean flux is significantly greater than 0  $\mu\text{g N}_2\text{O m}^{-2} \text{ s}^{-1}$  ( $p < 0.01$ ).

Flight date DD.HH	Area covered (km <sup>2</sup> )	Mean N <sub>2</sub> O flux ( $\mu\text{g N}_2\text{O m}^{-2} \text{ s}^{-1}$ )
25.18	90	0.05* (0.031, 0.082)
27.11	86	-0.01 (-0.035, 0.028)
27.19	22	0.015 (0.004, 0.032)
28.10	69	0.10* (0.068, 0.140)
28.15	44	0.04 (0.005, 0.080)
All flights	311	0.043* (0.025, 0.055)

15

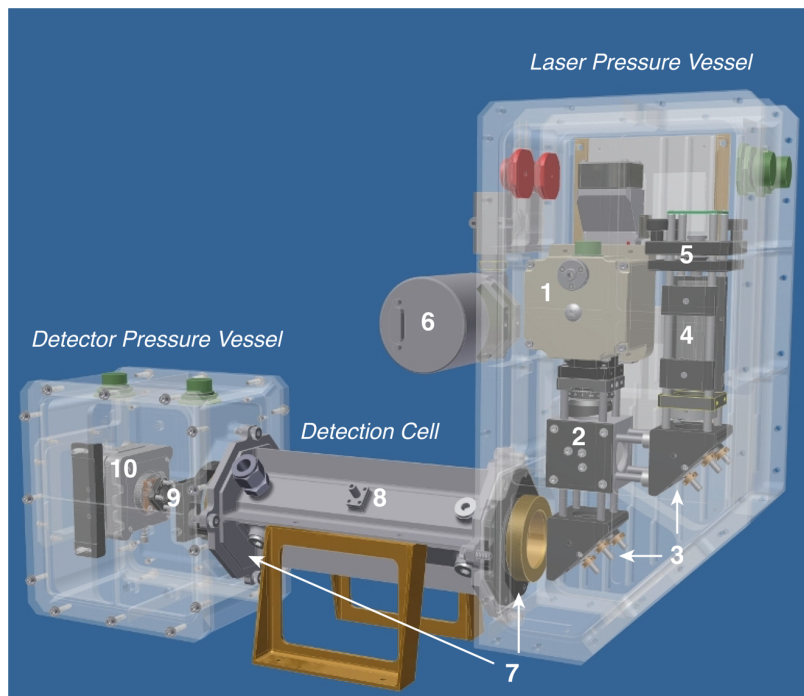


**Figure 4.** CAD model of N<sub>2</sub>O/CH<sub>4</sub>/H<sub>2</sub>O ICOS instrument shows 1) quantum cascade laser housing, 2) beam splitter, 3) steering optics, 4) Ge etalon, 5), etalon detector, 6) Baratron pressure sensor, 7) ICOS cavity mirrors, 8) temperature sensor port, 9) focusing optics, and 10) MCT detector. The detection cell is 25 cm long.

5

10

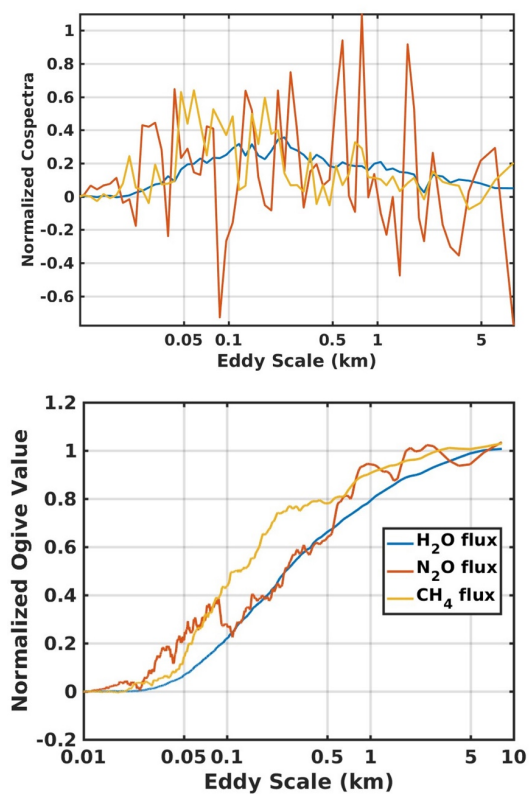


**Figure 5.** Normalized average cospectra and ogives for H<sub>2</sub>O flux, N<sub>2</sub>O flux, and CH<sub>4</sub> flux. The average covers the entire flight campaign. The ogive integration starts from the small eddy sizes.

5

Deleted: <object>

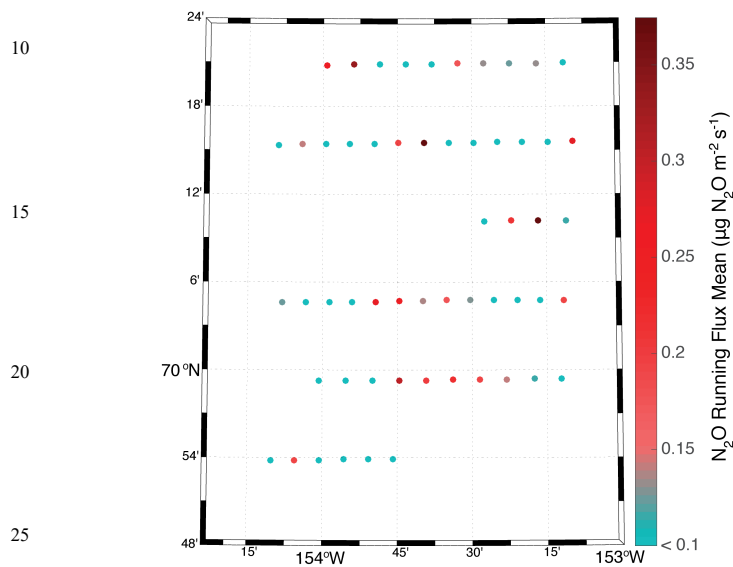
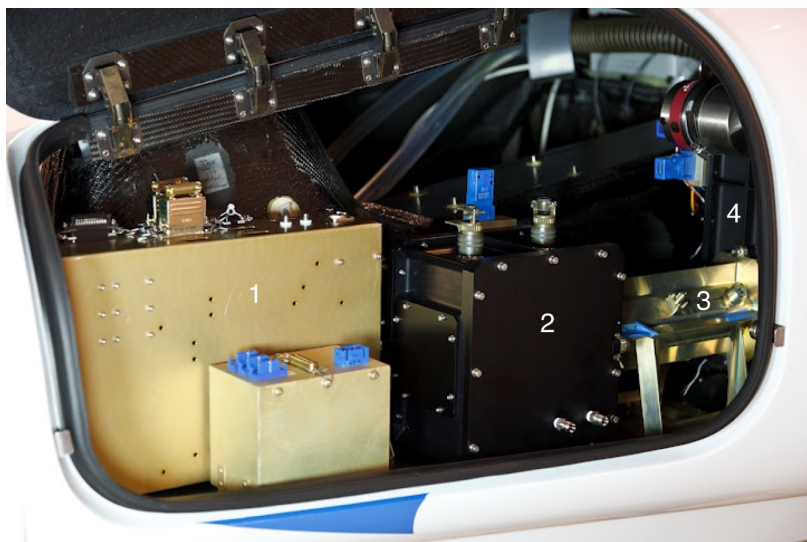


**Figure 6.** Spatial flux map for Flight 28.10, where the circles on the map each represent the N<sub>2</sub>O flux averaged over 6 km with 3 km overlap. Values within  $\pm 0.1 \mu\text{g N}_2\text{O m}^{-2} \text{s}^{-1}$  are treated as zero.

30



15 **Figure S1.** Image of N<sub>2</sub>O/CH<sub>4</sub>/H<sub>2</sub>O instrument in aircraft's luggage bay, which shows 1) electronics board, 2) detector  
pressure vessel, 3) detection cell, and 4) laser pressure vessel. Electronic cables were removed for clarity. ([Referenced in](#)  
20 [Section 2.2](#))

25

30

23

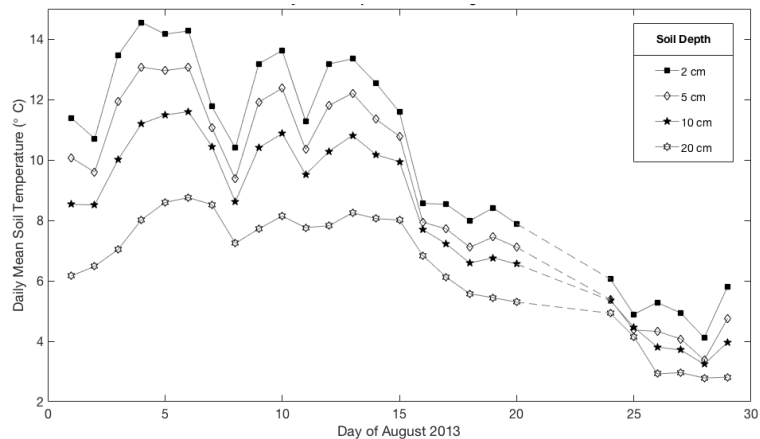


**Figure S2.** Daily mean soil temperatures at 2, 5, 10, and 20 cm depths. Each temperature shown is based on averaging 3 temperature probe sites located in the vicinity of the flux tower and then averaged for the full day. August 21-23 are missing because the flux tower platform was not being operated at that time. ([Referenced in Section 3.3](#))

5 **Table S1. In-flight precision and observed flux averages with 99% CI range.** Second column lists flight-by-flight precision from in-flight calibration data, [\(as determined by Eq. \(1\)\)](#). Spatially averaged fluxes are presented with bootstrap-derived 99% confidence intervals in parentheses. [\(Referenced in Sections 2.2 and 3.3\)](#)

Flight date DD.HH	$\sigma_{\text{N}_2\text{O}}$ (ppb Hz <sup>-1/2</sup> )	Mean N <sub>2</sub> O flux ( $\mu\text{g N}_2\text{O m}^{-2} \text{ s}^{-1}$ )
25.18	0.30	0.05 (0.016, 0.097)
27.11	0.53	-0.01 (-0.053, 0.045)
27.19	0.58	0.015 (-0.003, 0.040)
28.10	0.27	0.10 (0.049, 0.160)
28.15	0.44	0.04 (-0.002, 0.103)
All flights		0.043 (0.017, 0.063)

Deleted: .